AD-A139 750 THE OPTIMIZED ARCH DESIGN THEORY AND ENGINEERING PRACTICES(U) FOREIGN TECHNOLOGY DIV WRIGHT-PATTERSON AFB OH W SHENGLI 12 MAR 84 FTD-ID(RS)T-0114-84 1/1

UNCLASSIFIED F/G 13/13 NL

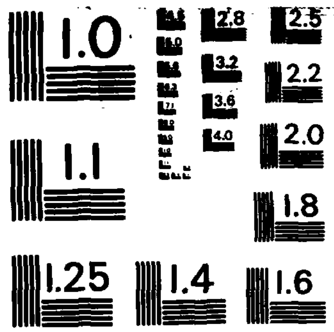

MICROCOPY RESOLUTION TEST CHART
NATIONAL BUREAU OF STANDARDS-1963-A

AD A139750

FTD-ID(RS)T-0114-84

FOREIGN TECHNOLOGY DIVISION

THE OPTIMIZED ARCH DESIGN THEORY AND ENGINEERING PRACTICES

by

Wang Shengli

DTIC FILE COPY

DTIC ELECTE APR 5 1984 S D

D

Approved for public release; distribution unlimited.

84 04 05 029

Accession For	
NTIS GRA&I	☒
DTIC TAB	☐
Unannounced	☐
Justification	
By	
Distribution/	
Availability Codes	
Dist	Avail and/or Special
A-1	

DTIC COPY INSPECTED 3

FTD-ID(RS)T-0114-84

EDITED TRANSLATION

FTD-ID(RS)T-0114-84 12 March 1984

MICROFICHE NR: FTD-84-C-000271

THE OPTIMIZED ARCH DESIGN THEORY AND ENGINEERING PRACTICES

By: Wang Shengli

English pages: 57

Source: Dixia Gongcheng, Nr. 9, 1982, pp. 1-15

Country of origin: China
Translated by: LEO KANNER ASSOCIATES
F33657-81-D-0264
Requester: FTD/SDBF
Approved for public release; distribution unlimited.

THIS TRANSLATION IS A RENDITION OF THE ORIGINAL FOREIGN TEXT WITHOUT ANY ANALYTICAL OR EDITORIAL COMMENT. STATEMENTS OR THEORIES ADVOCATED OR IMPLIED ARE THOSE OF THE SOURCE AND DO NOT NECESSARILY REFLECT THE POSITION OR OPINION OF THE FOREIGN TECHNOLOGY DIVISION.	PREPARED BY: TRANSLATION DIVISION FOREIGN TECHNOLOGY DIVISION WP.AFB, OHIO.

GRAPHICS DISCLAIMER

All figures, graphics, tables, equations, etc. merged into this translation were extracted from the best quality copy available.

THE OPTIMIZED ARCH DESIGN THEORY AND ENGINEERING PRACTICES

Wang Shengli

I. General Discussion

Early, during the beginning of the 1950's, C.C. Daweiduofu, in his book entitled "The Calculation and Design of Underground Structures" wrote: "By studying these results, we can conclude that the work strength of an integral underground structure is not attained by enlarging the thickness of the section and excessive costs of the materials but by selecting a very good lining shape and determining a rational ratio between the component dimensions." A large amount of practice shows that whether or not this excellent lining shape (i.e. the optimized arch shape) has great influence on the internal force and deformation of the structure as well as the engineering firmness and economy [2-6]. Therefore, the optimized arch shape design has been given serious attention both domestically and abroad. However, to date, we are still lacking a fast, convenient, accurate and practical method to implement the optimized arch shape design.

To implement the optimized arch shape design, it is not only necessary to have qualitative inferences but it is even more necessary to have a method with specific qualitative analysis; not only should the precision of the calculations satisfy construction requirements but it should also be simple and easy to carry out and convenient to use. In recent years, both domestically and abroad, the photoelastic method [7-8], the simulated material test method [9-10], the finite element calculation method [7], the engineering testing method [11], the elastic theory analysis method [5,12] and the internal force analysis method [1,13-15] have been used in a great deal of research on the rationality of arch shapes under certain specific conditions.

Yet, the common points of these methods are: they first establish one or several types of arch shapes and afterwards test and verify the rational load suitable for this arch but they do not begin from the different load distributions to find the optimized arch shape suitable for the different loads. Because the tests or calculated arch types and quantities were limited, they were unable to cover all of the various types of arches existing in actual engineering. Because of this, there is still a gap for its widespread use. For example, the elastic theory was used to study the rational loads of holonomic circles and holonomic ellipses under four-way stress conditions yet a part of the arch in actual engineering is often circular or elliptical and moreover the majority must consider three-dimensional stress. Thus, under these conditions, how should we determine the optimized arch shape? Research of the elastic theory on straight wall circular arches is only limited to analyzing the stress conditions of several known arch shapes and it is still unable to resolve the problem of how to find the optimized arch shape under different load distributions.

Naturally, on the basis of various research achievements, many authors [4,7,16-18] have carried out comprehensive discussions on the relationship of load and optimized arch shape and pointed out certain optimized arch shapes under specified loads. Without a doubt, it provides a train of thinking and convenience for the optimized arch shape design. However, these qualitative discussions are still unable to universally guide the optimized arch shape design work. For example, the book entitled Static Force Calculations of Underground Structures [16] proposed: "When the entire span of the arch sustains a vertical even distributed load, it is better to use the parabolic arch axis. When the arch only sustains the radial evenly distributed load, it is better to use the single centered circular arch. When the arch sustains an arbitrary load and the rise and span are fixed,

it is better to use a three-centered arch axis. Because we can use the sizes of varying radii R and r, the arch axis can as much as possible approach the stress curve." However, how do we change the size of R and r based on the changes of the load? There is no method brought forth in the book and therefore this problem requires further study to be resolved.

In the past and at present, China has continued to use the checking computations method [19-21]. This method which has many repetitions of checking computations is very complex and time consuming. Therefore, it greatly limits the initiatives of design personnel and causes some underground engineering designs to only consider satisfying the strength requirements but not to consider whether or not the arch shape is optimized. This results in undeserved waste and even fractures and breaking.

Abroad, Mositekefu summarized research design tests of large area underground structures in the modern Soviet Union [7] and proposed that when the top and sides sustain evenly distributed loads, we should not consider the approximate rational axis of the crushing of the arch - the rope curve (this is identical to the egg-shaped curve proposed by the Wuhan Institute of Hydroelectric Power [22]). When this curve is used to carry out optimized arch shape design, it is necessary to first draw the arch diagram point by point based on the curve equation and then based on the graphic method test select the center of the circle and radius so as to attain the multicentered circle's approximate theoretical curve. This method reduced the blindness of assuming the calculations which is naturally a big step forward. Yet, it is unable to organically integrate the optimized arch shape with its corresponding curvature radius, position of the center of the circle and oblique angle of the control section etc. It requires artifical test selected circle centers and radii and therefore the artificial discrepancy is relatively large. Even if we use test drawing to obtain the optimized arch

shape indicated by a multicentered circle, as soon as it is in contradiction with the service clearance and construction requirements, it is difficult to resolve the overall plan. Therefore, even Mositekefu himself considers that: "We are often unable to use the most advantageous sectional form of the static load conditions based on the construction conditions." He finally concluded that: "In the majority of situations, when considering the convenience of the construction conditions, the contour of the large span arch axis should use the circular curve [7]." Is this circular curve a single centered circle or multicentered circle? How is its optimized radius determined? If it is a multicentered circle then where should its curvature's changing points be? If it is a straight wall single centered circular arch, how do we select its optimized vector-span and rise-span ratios? These problems have not yet been resolved and therefore we are still unable to effectively guide engineering practices.

The method proposed in this paper is a method which, on the basis of resolving the above problems, attempts to find the optimized arch shape by emphasizing the solution of the common seen loads of underground engineering. The main features of this method are: (1) it has fast speed and is simple and convenient. By using an electronic computer for about 10 minutes we can obtain an optimized arch shape which raises the work efficiency several tens of times more than the check computation method. (2) It can provide at one time several different optimized arch shape plans which is convenient for designers to carry out technical and economic comparisons and select a feasible plan which has rational stress, saves on investment, is convenient for construction and can satisfy the service requirements. (3) When test data on the stratigraphical stress is lacking, based on the actual arch shapes of constructed projects and their destruction conditions, we can also deduce their load distribution pattern to provide data for engineering rebuilding,

continued building and stratigraphical comparisons.

Practice has proven that by using the optimized arch shape design, we can cause the structural thickness to become noticeably thinner under the same load and safety coefficient and thus lower the engineering costs; or under the same conditions of materials depletion (or decreasing the materials depletion), we can effectively reduce or eliminate the production of fractures and thus raise the engineering quality. This economical method is simple, convenient and easy to implement, does not require expending capital construction investments and it can obtain marked economic effects. Following the daily increases in underground construction and advancements towards large spans, these economic and technical effects are becoming increasingly noticeable. At the same time, following the advancements in ground pressure research and measurement technology, optimized arch shape designs have also been gradually perfected. There is no doubt that this is of important significance for the faster and more economical development of underground structures.

II. Fundamental Method

(1) Curved Wall Lining Optimized Arch Shape Design

1. Establishing the arch shape's basic calculation equation, the relationship of the arch's key elements and the arch's shape.

Everyone knows that the arch shapes commonly used in engineering are semi-circles, cyclotomic ellipses, three centered circles, parabolas, catenary, horseshoe arches etc. (Fig. 1).

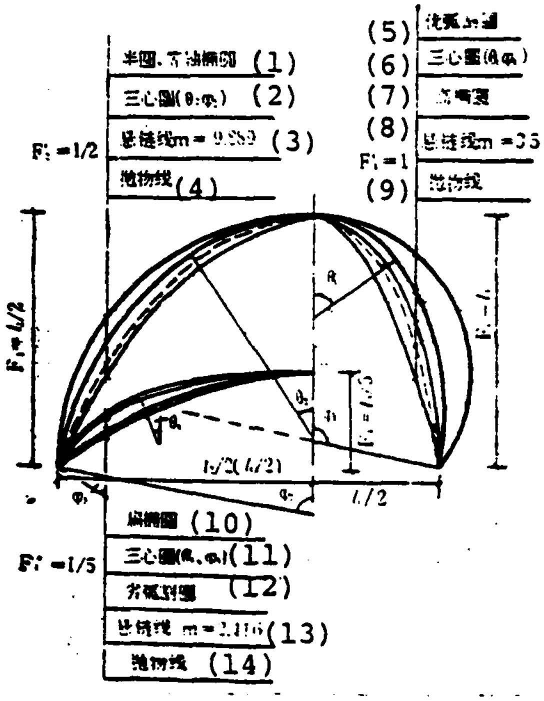

Fig. 1 Arch shapes commonly used in engineering.

Key: (1) Semi-circle, isometric ellipse; (2) Three-centered circle; (3) Catenary; (4) Parabola; (5) Major arc cyclotomic; (6) Three-centered circle; (7) High ellipse; (8) Catenary; (9) Parabola; (10) Oblate ellipse; (11) Three-centered circle; (12) Minor arc cyclotomic; (13) Catenary; (14) Parabola.

Then what generalities and characteristics do these arch shapes have? What are the differences and connections between them? What mathematical formula is used to express the many unknown arch shapes among the various known arch shapes?.....If we lack unified arch shape calculation formulas and comparative quantities, the above questions are difficult to answer. In order to investigate the relationships of the quantitative changes to qualitative changes between the arch shapes, we introduced a type fundamental quantity to determine the quality of the arch shape - the arch shape's key elements (F, l, θ, φ) and with these key elements we can use a general formula to express or

approximate the various arch shapes. In considering the convenience of the design and construction, below we use the three-centered circle as the basic system (Fig. 2).

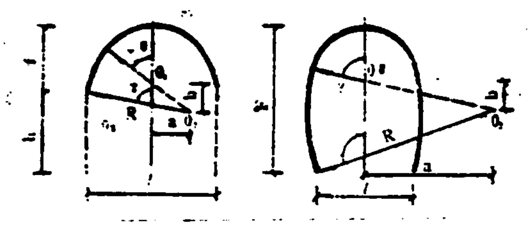

Fig. 2 Reference diagrams of arch structures.

When we know the arch's key elements, F,l, θ and φ, then $R=(F-K_1 l/2)/K_2$.

In the formula

$$\left.\begin{array}{l} K_1 = tg(\theta/2),\ K_2 = \sin\varphi[tg(\varphi/2) - K_1] \\ a = R\sin\varphi - l/2,\ b = a \cdot ctg\theta \\ r = R - a/\sin\theta \end{array}\right\} \quad (1)$$

This is the arch's basic calculation formula. In the formula:

F and l are separately the rise and span which can be determined by the service requirements.

θ and φ are separately the included angles between final point section and vertical line of the first and second circular arcs which can be determined based on the load distribution and vector-span ratio.

r and R are separately the radii of the first and second circular arcs.

a and b are separately the horizontal and vertical distances between the first circle center and second (third) circle center.

By substituting the F_o, l_o and φ_o of the inner contour into formula (1), we can obtain the inner contour's related dimension R_o, r_o, a_o and b_o. In the same way, by substituting F,l and φ of the inner contour (or F_1, l_1 and φ_1 of the outer contour) into formula (1), we can obtain the related dimensions of the axis (or outer contour). After the θ value is determined under load distribution conditions, it is a constant and therefore the θ value does not change when calculating the inner, outer or axis contour.

F and l (F_1, l_1) can be found based on the designed top thickness of the arch d_o and springer thickness of the arch d_n. Based on formula (2) we find

$$\left.\begin{array}{l}
(1)\ \text{轴线跨度}\ l = l_0 + d_n \cdot \sin\varphi_0 \\
(2)\ \text{轴线矢高}\ F = F_0 + d_0/2 - d_n/2 \cdot \cos\varphi_0 \\
(3)\ \text{外轮廓跨度}\ l_1 = l + d_n \cdot \sin\varphi_0 \\
(4)\ \text{外轮廓矢高}\ F_1 = F + d_0/2 - d_n/2 \cdot \cos\varphi_0
\end{array}\right\} \quad (2)$$

Key: (1) Axis span; (2) Axis rise; (3) Outer contour span; (4) Outer contour rise.

In the formulas, l_o and F_o separately indicate the clear span and clear rise.

The method for finding θ and φ (φ_o, φ_1) is described in detail in the book entitled <u>Determination of the Key Elements of the Optimized Arch</u>.

It can be proven that when the arch's key elements θ and φ and vector - span ratio F' use different numerical value combinations,

it can express or approach the various different arch shapes (Fig. 3). When $\theta \approx$ arctg2.2F' and φ =arctg4F', it approaches a parabola (the bottom curve in the figure) and each point on the line represents a different parabolic arch shape, for example, 1, 2, 3 and 4. When φ =arctg2F' and θ=45° (the upper line in the figure), it is a circular arc line and each point on the circular arc line represents a different cyclotomic or semi-circle such as 8, 12, 13 and 14 in the figure. When θ=arctg2F' and φ =90°, it indicates a semi-elliptical line and each point on the line indicates an oblate semi-ellipse, high semi-ellipse or isometric ellipse such as 6, 7, 8 and 20 in the figure. The vector-span ratio of the point where the isometric ellipse and semi-circle intersect is F'=0.5 and when separately substituted into the circular arc line or semi-elliptical line arch shape's key elements calculation formula, we can find similar arch shape key elements. That is, when θ =45° and φ =90°, this explains that the isometric ellipse is a semi-circle. We can see from Fig. 3 that when F' $<$ 1/2, the semi-elliptical line is above the circular arc line and when F' $>$ 1/2, the semi-elliptical line is below the circular arc line and the parabola is always below the circular arc line and semi-elliptical line. However, the smaller F', the closer the circular arc line and semi-elliptical line; the larger F', the closer the semi-ellipse and parabola. This completely coincides with the actual arch shape when in Fig. 1.

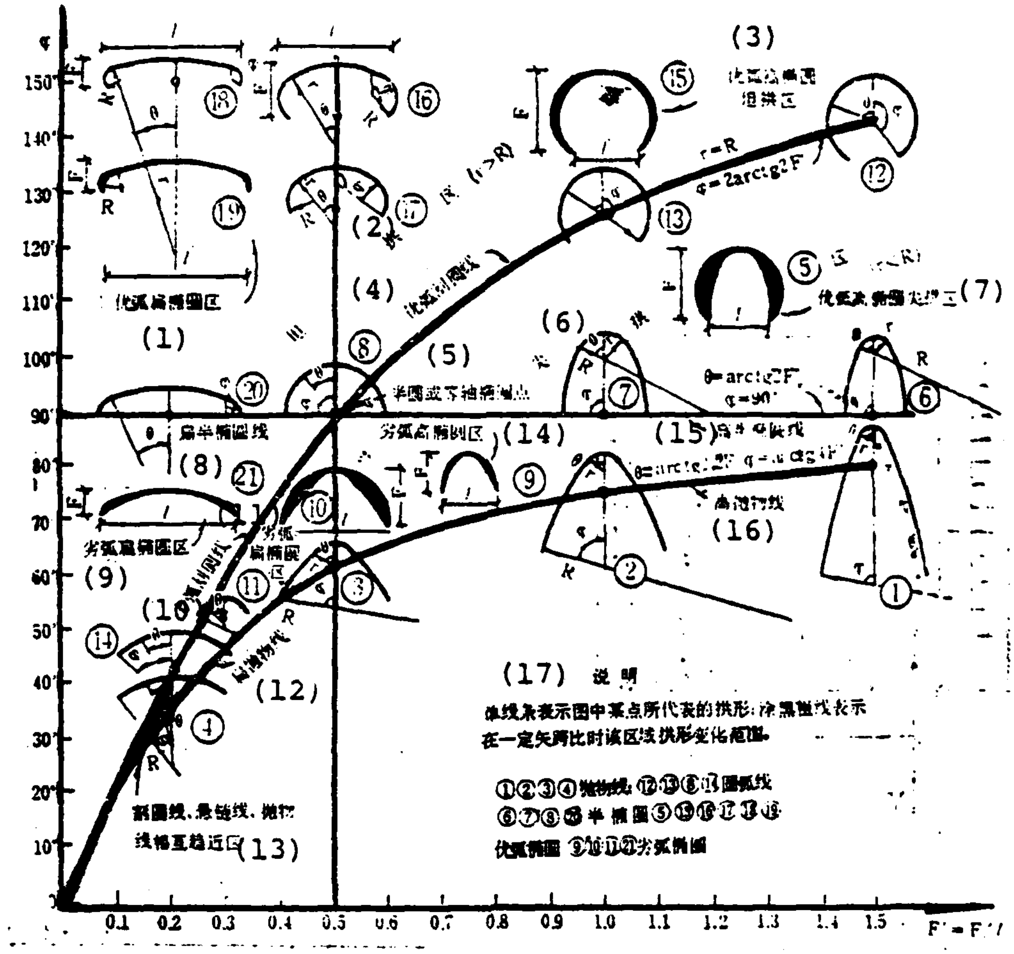

Fig. 3 Relationship of changes of the arch shape's key elements and the changes of the arch shape.

Key: (1) Major arc oblate ellipse area; (2) Depressed arch area; (3) Major arc high elliptic depressed arch area; (4) Major arc cyclotomic line; (5) Semi-circular or isometric elliptic point; (6) Pointed arch area ; (7) Major arc high elliptic pointed arch area; (8) Oblate semi-elliptic line; (9) Minor arc oblate elliptic area; (10) Minor arc cyclotomic line; (11) Minor arc oblate elliptic area; (12) Oblate parabola; (13) Mutual approach area of cyclotomic line, catenary and parabola; (14) Minor arc high elliptic area; (15) High semi-elliptic line; (16) High parabola; (17) Explanations: a single line indicates an arch shape represented by certain points in the figure; the black thick lines indicate the change range of the area's arch shape when in a certain rise-span ratio; 1, 2, 3 and 4 are parabolas; 12, 13, 8 and 14 are circular arc lines; 6, 7, 8 and 20 are semi-ellipses; 5, 15, 16, 17, 18 and 19 are major arc ellipses and 9, 10, 11 and 21 are minor arc ellipses.

Any one point $M(F', \varphi)$ on Fig. 3 represents a specific arch shape. The different points then represent different arch shapes. The collection of many points with the same characteristics form an arch shape area, for example, the depressed arch area (this is a collection of arch shapes with innumerable $r > R$. It includes the major arc high elliptic depressed arch area and major arc or minor arc oblate elliptic depressed arch area) and the pointed arch area (this is a collection of arch shapes with innumerable $r < R$. It includes the minor arc oblate elliptic pointed arch area and major arc or minor arc high elliptic pointed arch area etc.). They use the circular arc line (mostly $r=R$ arch shape collections including major arc cyclotomic, minor arc cyclotomic and semi-circles) as the boundary line. Based on the names of the separate arch shape areas, we can know the generality of the area's arch shape. For example, the major arc oblate elliptic depressed arch area indicates an arch shape area wherein the arc length is greater than the semi-ellipse's arc length, the vector-span ratio is smaller than 1/2 ($F' < 1/2$) and the radius of the first circular arc is larger than the radius of the second circular arc ($r > R$); the minor arc high elliptic pointed arch area indicates an arch shape area wherein the arc length is smaller than the semi-elliptic arc length, $F' > 1/2$ and $r < R$; and the cyclotomic, parabola and catenary approaching areas signify three mutually close arch shape areas (Fig. 3). Calculations show that when $F' \leqslant 1/5$, the longituding coordinate error of the circular arc and its corresponding catenary does not exceed 1.7% (the corresponding catenary is the catenary with the arch axis coefficient $m=1/2[F/(1-y_{1/4})-2]^2-1$ and $y_{1/4}$ is the longitudinal coordinate of the circular arc in the arch span 1/4 point); when $F' \leqslant 1/10$, the maximum errors of the longitudinal coordinates of the two do not exceed 1/1900 and is also very close to the parabola. However, in the same arch shape area, the arch shape of each point is not completely the same and all have slight differences indicating the intrinsic individuality of this point's

arch shape. If we can find the longitudinal coordinates (F', φ) of the optimal arch shape point based on the load size and distribution etc. factors, then we can conveniently obtain the optimixed arch shape suitable for this load situation.

2. Determination of the key elements of the optimized arch shape - relationship of the load and optimized arch shape.

The optimixed arch shape is an arch shape which can cause, under certain load effects, the bending moment of each section to the minimum and even zero. The horizontal coordinates use the arch's springer center and the longitudinal coordinates use the vertical line of the vault. See Fig. 4 for the calculation diagram.

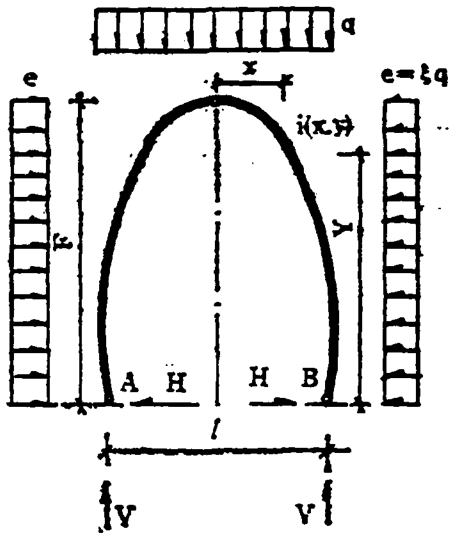

Fig. 4 Calculation diagram of optimized arch shape equation.

We can deduce the optimized arch shape equation from the principles of mathematical mechanics as follows:

$$x^2+\xi y^2+yl^2/4F-\xi Fy-0.25l^2=0 \qquad (3)$$

In the formula, ξ is the lateral pressure coefficient and ξ =e/q.

The arch shape which satisfies the optimized arch shape equation can cause the bend moments of the sections of the three-hinged arch to be zero and although it is unable to create the ideal condition for the hingeless arch etc. of the bending moment of each section's constant load being zero (the reason for this is simply that the axial force effects in the deformation of the arched structure are small), yet it is not equal to zero. However, by using other curves as the arch's axis there is a greater possibility of making the constant load's bending moment of each section zero [23]. Therefore, use of the above optimized arch shape equation is still the most appropriate. By doing it this way, we can cause the constant load's bending moment to decrease to the lowest limit yet it still can be regarded as an optimized arch shape.

Below we further analyze that when $\xi=0$, formula (3) becomes

$$y=(1-4x'^2)F \qquad (4)$$

In the formula, $x'=x/l$. This is a parabolic equation and explains that its optimized arch shape is a parabola only when there is a vertical evenly distributed load. It can be approached by using the three-centered circle with $\theta \approx \operatorname{arctg}2.2F'$ and $\varphi=\operatorname{arctg}4F'$.

In actual engineering, the lateral pressure is never zero. At this time $\xi>0$ and then formula (3) can be simplified as:

$$x^2/A^2+(y-E)^2/B^2=1 \qquad (5)$$

In the formula:

$$E=F/2-l^2/8F\xi,\quad B=F-E,$$
$$A=B\sqrt{\xi}.$$

This is an elliptic equation. It is the optimized arch shape equation when there are the joint effects of vertical evenly distributed load and laterially and even distributed load.

We can know by using the geometric chart making method from a mathematics handbook [24] that by using the circular arc method we can approximately make an elliptic diagram (5).

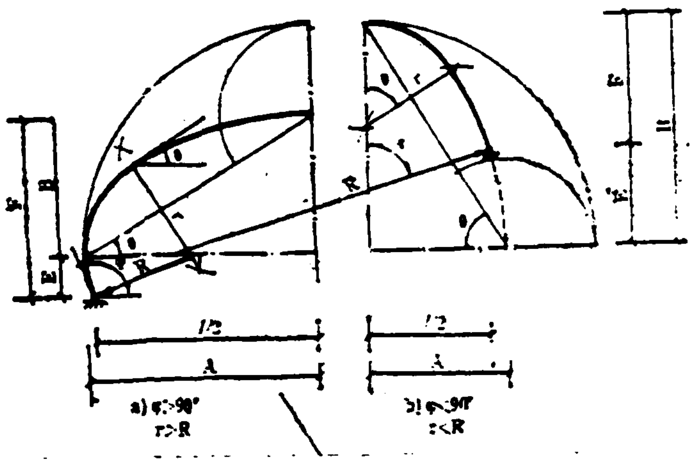

Fig. 5 Calculation diagram of arch shape's key elements.

Based on the arch shape's basic calculation formula and the geometric relations in Fig. 5, we can obtain

$$\left.\begin{aligned}
\theta_{(1)} &= \text{arc tg}\,(B/A) = \text{arc tg}\,(1/\sqrt{\xi}) \\
\varphi_{(2)} &= \text{arc cos}\left\{\left[\left(1-\text{tg}\frac{\theta}{2}\right)/\left(1-\sqrt{\xi}\,\text{tg}\frac{\theta}{2}\right)\right]\cdot\right. \\
&\quad \left.\cdot\cos 2\left[\text{arc tg}\,(2\sqrt{\xi}F')\right]\right\} \\
&= \text{arc cos}\left\{\left[(1-K_1)/(1-\sqrt{\xi}K_1)\right]\cdot\right. \\
&\quad \left.\cdot\left[(1-4\xi T'^2)/(1+4\xi F'^2)\right]\right\}
\end{aligned}\right\} \quad (6)$$

Key: (1)-(2) Optimized.

In the formula, $K_1=tg(\theta/2)$. After obtaining $\theta_{optimized}$ and $\theta_{optimized}$ from formula (6), we can obtain each of the optimized arch shape's related dimensions calculated according to the arch shape's basic calculation formula (1). In actual engineering design, we can also use Fig. 6 to directly find the optimized arch shape's key elements θ and φ. The method is

to make a vertical line according to a known vector-span ratio F' which intersects with the lateral pressure coefficient ξ at one point. From this, the intersecting point which goes from the horizontal line to the longitudinal coordinate area can be read as the φ value. Moreover, the ξ line can be read as the θ value.

Under special situations, when the vertical evenly distributed load and horizontal laterally and evenly distributed load are equal, ξ =1 and formula (60 can be simplified into

$$\theta_{optimized}=\text{arc tg}(1/\sqrt{1})=45°$$

$$\varphi_{optimized}=2\text{arc tg}2F'$$

It shows that the optimized arch shape is the circular arc (major arc cyclotomic, minor arc cyclotomic or semi-circle) when the vertical and lateral evenly distributed loads are equal.

3. The curved wall lining optimized arch shape design method - relationship of the load and optimized arch shape.

Above, we established the relationships of the arch shape and arch shape's key elements and that of the load and arch shape's key elements. Then, by further using the arch shape key elements as the bridge, we can establish the relationship of the load and the optimized arch shape. In essence, the design of the curved wall lining optimized arch shape obtains the optimized arch shape's key elements based on the load and then solves the optimized arch shape. The method is very simple. The specific steps are:

(1) Based on loads q and e computed from the actual measurements or related design standards, we find laterial pressure coefficient ξ ; we find rise-span ratio F'=F/l based on

span l and rise F determined from the service requirements.

(2) Based on ξ and F' we obtain θ and φ from formula (6) or directly find the optimized arch shape's key elements θ and φ from Fig. 6.

(3) By substituting a known value into formulas (1) and (2), we can obtain the related dimensions of the optimized arch shape and then draw the optimixed arch shape diagram.

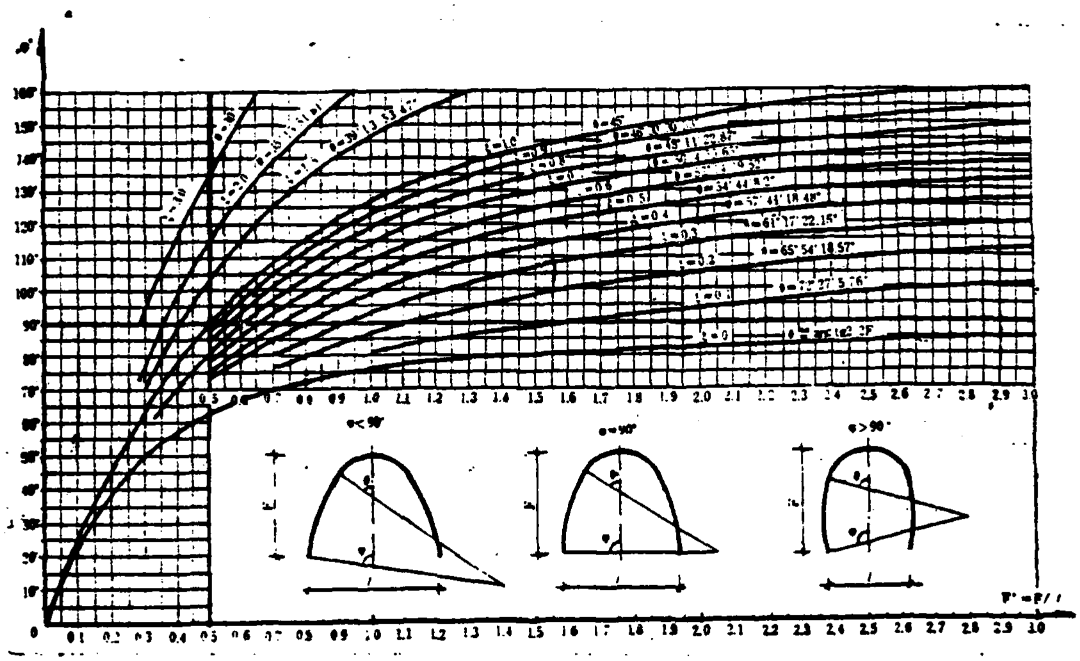

Fig. 6 Diagram of the selection of the curved wall lining optimized arch shape's key elements.

When ξ =1, formula (1) changes into a very simple form because when ξ =1 then φ =2arc tg2F'

$$\therefore R = r = \frac{l}{2\sin\varphi} \qquad a = b = 0 \cdots\cdots (1-1)$$

Sometimes, for artistic requirements, we can also first determine the φ value. Optimized vector-span ratio F' is

obtained based on φ and ξ from Fig. 6 and afterwards we substitute in formula (1) and (2) and obtain the optimized arch shape. For example, when the arch is constructed according to the semi-ellipse, by taking φ =90° we can then obtain optimized vector-span ratio $F'=1/2\sqrt{\xi}$ from formula (6) (naturally, it can also be looked up in Fig. 6) and the basic calculation formula of the arch shape can be simplified as:

$$\left.\begin{aligned} &R=(F-0.5K_1l)/(1-K_1)\\ &a=R-0.5l\\ &b=a\cdot\mathrm{ctg}\theta\\ &r=R-a/\sin\theta\\ &\text{式中}\theta=\mathrm{arctg}\xi^{-1/2}\qquad K_1=\mathrm{tg}(\theta/2)\end{aligned}\right\}(1-2)$$

(1)

Key: (1) In the formula.

The curved wall arch shape structure designed according to the optimized arch shape basically does not have bending moment or only has very small bending moment and therefore this can be disregarded. Thus, it also does not produce elastic resistance. Therefore, we can only consider the effects of the axial pressure which causes the calculations of the inner force and sections to become very simple.

Example 1: a certain known tunnel has a clear width of 4.9 meters, a clear height of 7 meters, lateral pressure coefficient ξ =0.4 and we try to find the inner contour dimensions of the curved wall optimized arch shape.

(1) (2) (3)

$$\text{已知}\ l_0=4.9\text{米},\ F_0=7\text{米},\ \therefore F_0'=F_0/l_0=7/4.9=1.4826$$

$$\xi=0.4$$

Key: (1) Known; (2)-(3) Meters.

(1)
解 $\theta = \mathrm{arc\,tg}\,\xi^{-1} = 54°41'18.48'' \approx 57.7°$

$$K_1 = \mathrm{tg}(\theta/2) = 0.5508$$

$$\varphi_0 = \mathrm{arc\,cos}\left\{\left[(1-0.5508)/(1-\sqrt{0.4}\times 0.5508)\right]\left(\frac{1-4\times0.4\times1.4286^2}{1+4\times0.4\times1.4286^2}\right)\right\}$$

$$= 111.4761°$$

Key: (1) Solution.

(θ and φ can also be directly looked up in Fig. 6).

$$K_2 = \sin\varphi[\mathrm{tg}(\varphi/2) - K_1] = 0.8536$$

$$R_0 = (F_0 - 0.5K_1 l_0)/K_2 = 6.6200 \text{米}\ (1)$$

$$a_0 = R_0 \sin\varphi_0 - 0.5l = 3.7104 \text{米}\ (2)$$

$$r = R_0 - a_0/\sin\theta = 2.2298 \text{米}\quad (3)$$

$$b = a_0\ \mathrm{ctg}\theta = 2.3467 \text{米}\quad (4)$$

Key: (1)-(4) Meters.

Its arch shape is as shown in Fig. 7.

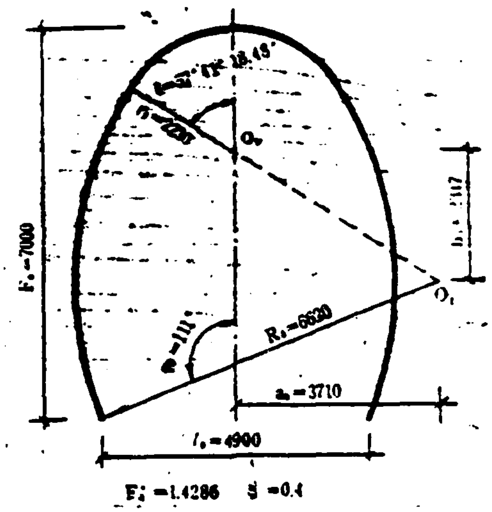

Fig. 7 Inner contour of optimized arch shape.

In the same way, if it is necessary to calculate the contour of the axis or the outer contour, we can still calculate

according to the above mentioned method. However, only rise F, span l and angle φ are different. If the sections are constant sections or the variable sections do not have large changes in thickness, we can also assume that the φ angle does not change and its error is very small.

Example 2: the strata pressure measurement results of a certain two line tunnel on the southern section of the Beijing-Guangzhou line are: the mean value of the lateral pressure is nearly equal to that of the vault and when it is slightly larger than the pressure of the vault we can approximately take ξ =1[25], find the optimized arch shape during its construction and compare it with the pressure curve calculated from the measured data. The maximum measured load of this tunnel is 41.4 tons/meter^2 and we attempt to estimate the thickness of the structure.

We can know from the figures in this paper that this tunnel's outer contour rise F_1=10.85 meters, external span l_1=13.1 meters and $\therefore F_1'=F_1/l_1=0.8282$.

When ξ=1, it can be directly solved by formula (1-1):

$$\varphi_1=2\mathrm{arc\ tg}(2F_1')=117.7624°$$

Therefore, $R_1=l_1/2\sin\varphi_1=6.1307$ meters

When we estimate the thickness of the section, we can calculate the axial force based on the following formula:

$$N \approx qR_1 \approx 253.81 \text{ tons}$$

When using Number 150 concrete, its axis compressive strength R_a=850 tons/meter^2. Based on the provisions of the "Tunnel Stipulations," when using compressive strength control under main load effects, safety coefficient K is taken as 2.4.

$$\therefore d=NK/R_a \approx 0.717 \text{ meters, taken as } 0.75 \text{ meters}$$

If we use constant sections, then axis radius $R=R_1-0.75/2=$ 5.7287 meters. Inner contour radius $R_o=R_1-0.75=5.3537$ meters.

When we consider the effects of non-uniform load distribution, pressure fluid and seasonal underground water on strata pressure, we can use reinforcing bars based on the structure.

The above mentioned optimized arch axis is as shown in Fig. 8 and when compared to the pressure curve made in the bending moment diagram which was calculated from the actually measured strain value of this engineering, their regularities are completely identical. The optimized arch shape curve is a major arc cyclotomic, the pressure curve is also an approximate major arc cyclotomic and the two have flatter vaults than that of the original design and the hances and toes are raised out a little more towards the outside. This is advantageous for preventing the observed vault from arching upwards, the inner rim of the vault from being crushed and destructive phenomena such as the hance and toes being pulled and cracked etc. Moreover, it causes the thickness of the structure to become thinner.

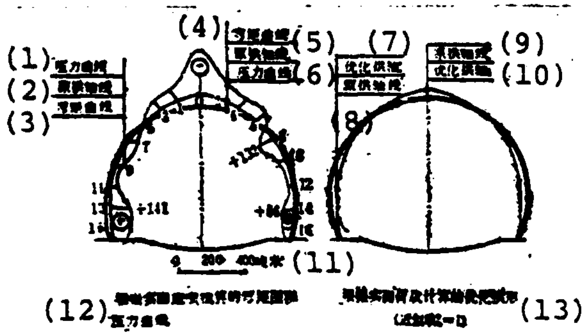

Fig. 8 Comparison of optimized arch axis, original arch axis and pressure line.

Key: (1) Pressure curve; (2) Original arch curve; (3)-(4) Bending moment curve; (5) Original arch curve; (6) Pressure curve; (7) Optimized arch axis; (8)-(9) Original arch curve; (10) Optimized arch axis; (11) 400 tons/meter^2; (12) Bending moment diagram calculated according to measured strain and pressure curve; (13) Optimized arch shape calculated according to measured load [approximately taken as =1].

(2) Straight Wall Lining Optimized Arch Design

In considering construction convenience and the full utilization of the interior space especially when the lateral pressure is not large, we often use the straight wall arched structure in engineering. The straight wall arched structure first considers construction and service requirements and although it cannot cause the bending moment of each section to approach zero as does the curved wall lining, yet under certain conditions by selecting a suitable vector-span ratio or rise-span ratio we can cause the bending moment of each section to be relatively small and the distribution to be relatively even thus attaining to rational economic goals.

1. Basic Formula for Calculating the Internal Force

Because the optimized arch shape with a straight wall arched structure still has certain bending moment and axial force, it is necessary to first fix certain conditions (e.g. the arch's shape, base form etc.), then calculate the internal force and afterwards make comparisons so as to be able to determine whether or not it is optimized. For this reason, below we will enumerate the basic formula for calculating the internal force:

$$M_i = \alpha_i \, ql^2 \qquad N_i = \beta_i \, ql \qquad (7)$$

In the formula, M_i and N_i are separately the bending moment and axial force of the i section. a_i and β_i are separately the bending moment coefficient and axial force coefficient of the i section.

$$\alpha_i = y'[\xi(B - y'/2) - A] + x_1'x_2'/2 + \alpha_{(1)}$$
$$\beta_i = [\xi(y' - B) + A]\cos\psi + (1/2 - x_1')\sin\psi$$

Key: (1) Springer.

A and B separately indicate the arch shape and base form

effect coeficients under vertical uniform load and lateral uniform load. Their values are equal to the ratio of the arch springer's horizontal thrust and ql which can be looked up in structural manuals or directly calculated.

$a_{springer}$ is the arch springer's bending moment coefficient and the arch springer's bending moment coefficient of the hingeless arch can be looked up in or calculated from a structural handbook. The $a_{springer}$ of three-hinged arches and double-hinged arches are zero. See Fig. 9 for details on the other arches.

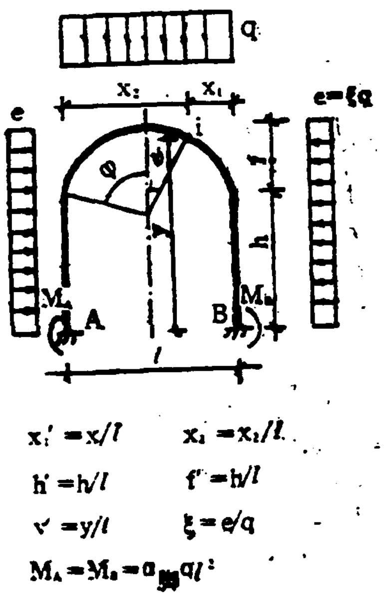

(I)

Fig. 9
Key: (1) Springer.

We can use formula (7) to calculate the internal force of arbitrary sections of straight walls, curved walls, arbitrary arch shapes (cyclotomic, semi-circle, elliptic, parabolic etc.) and arbitrary base forms (hingeless, double-hinged and three-hinged). Only A, B and $a_{springer}$ are different.

For example: the brick, concrete etc. straight wall vault

structures commonly used in civil air defense engineering are generally analyzed based on the constant section double hinged straight wall circular arch [26]. By using the force method to solve a statically indeterminate structure, we can obtain the A and B coefficient values of the constant section double hinged straight wall cyclotomic arch

$$
\begin{aligned}
A &= \frac{\eta_5/4 - \eta_3 h'\sin\varphi/2}{8h'^3\sin^4\varphi/3 + 4\varphi h'^2\sin^3\varphi + 4\eta_1 h'\sin^2\varphi + \eta_2\sin\varphi} \\
B &= \frac{h'^4\sin^4\varphi + 2\varphi h'^3\sin^3\varphi + 3\eta_1 h'^2\sin^2\varphi + 1.5\eta_2 h'\sin\varphi + \eta_6/4}{8h'^3\sin^4\varphi/3 + 4\varphi h'^2\sin^3\varphi + 4\eta_1 h'\sin^2\varphi + \eta_2\sin\varphi}
\end{aligned}
\qquad (8)
$$

In the formula

$$
\begin{aligned}
&\eta_1 = \sin\varphi - \varphi\cdot\cos\varphi \\
&\eta_2 = 0.5\varphi - 1.5\sin\varphi\cos\varphi + \varphi\cdot\cos^2\varphi \\
&\eta_3 = -0.5\varphi - 0.5\sin\varphi\cos\varphi + \varphi\cdot\cos^2\varphi = \eta_2 - \varphi \\
&- \sin\varphi\cos\varphi \\
&\eta_4 = (0.5\varphi - 0.5\sin\varphi\cos\varphi)\cos\varphi \\
&\eta_5 = \eta_1\sin^2\varphi + \eta_4 - \sin^3\varphi/3 \\
&\eta_6 = 2\eta_1/3 - \eta_2\cos\varphi - 2\eta_4/3
\end{aligned}
$$

When it is a constant section double hinged semi-circular arch structure:

$$
\because \varphi = \pi/2 \quad \therefore \sin\varphi = 1,\ \cos\varphi = 0,\ \eta_1 = 1,\ \eta_2 = \pi/4
$$

$$
\eta_3 = -\pi/4,\ \eta_4 = 0,\ \eta_5 = 2/3,\ \eta_6 = 2/3 \text{ 代入 } (8)
$$

(1)

Key: (1) Substituted into.

The formula has

$$
\left.
\begin{aligned}
A &= \frac{\pi h'/8 + 1/6}{8h'^3/3 + 2\pi h'^2 + 4h' + \pi/4} \\
B &= \frac{h'^4 + \pi h'^3 + 3h'^2 + 3\pi h'/8 + 1/6}{8h'^3/3 + 2\pi h'^2 + 4h' + \pi/4}
\end{aligned}
\right\} (8-1)
$$

When it is a constant section double hinged drop circular arc arch:

$$
\begin{aligned}
\because h' = 0 \quad \therefore A &= \eta_5/(4\eta_2\sin\varphi) \\
B &= \eta_6/(4\eta_2\sin\varphi)
\end{aligned}
\qquad (8-2)
$$

When it is a constant section double hinged drop semi-circular arch:

(1)

$$\because \varphi=\pi/2 \therefore \eta_5=\eta_6=2/3 \quad \eta_2=\pi/4 \quad \sin\varphi=1 \text{ 且 } h'=0$$

Key: (1) Moreover.

By substituting in formula (8), we can obtain

$$A=B=2/3\pi \approx 0.21221 \qquad (8-3)$$

The springers of the above mentioned structural arches are all hinge supported and therefore all of the $a_{springer}$ are zero. In the same way, we can obtain the A, B and $a_{springer}$ values of the hingeless arch or three hinged arch, the constant section or variable section, with straight wall or without straight wall, circular arc or parabolic arches etc. By substituting in formula (7), we can obtain the bending moment axial force.

2. Internal Force Line Calculation Graph

We can know from the internal force calculation formula that the arch shape, base form, rise-span ratio, vector-span ratio, change law of the section's thickness, lateral pressure coefficient as well as the section's position etc. all influence the size and direction of the internal force. In order to use the relatively uniform optimized arch shape with small bending moment, we changed the many factor problem into a single factor problem. We first fixed certain conditions and afterwards found the relationship of the bending moment of each point on the cross section (e.g. the vault, hance, springer, wall etc.) and the axial force coefficient which changes with the lateral pressure coefficient from formula (7). This is the internal force line calculation graph.

Example: Figure 10 shows the internal force line calculation

graph of the constant section double hinged straight wall semi-circular arch when rise-span ratio h'=0.65.

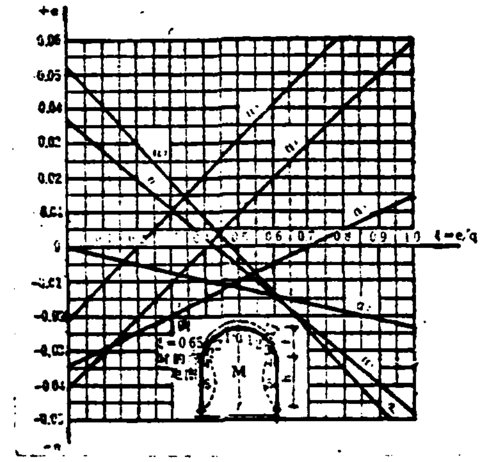

Fig. 10 Bending moment coefficient line calculation graph of double hinged straight wall semi-circular arch. Employed conditions: $n=d_o/d_n=1$; $f'=f/l=1/2$; $h/l=0.63$; i point bending moment $M_i=a_i ql^2$.

If the above mentioned conditions change then the line calculation graph also correspondingly changes. Appendix 9 of Reference (27) has completed over 100 internal force line calculation graphs of ten types of arches including the double hinged constant section circular arch, hingeless constant section circular arch, hingeless variable section semi-circular arch, double hinged variable section parabolic arch, hingeless constant section or variable section quadratic parabolic arch, constant section straight wall circular arch, variable section straight wall circular arch etc. and we will not go into details here. During use, we should pay attention to carrying out calculations by selecting line calculation graphs compatible with the engineering conditions. Its usage and special features are:

(1) When using the line calculation graph to solve each section's internal force, it is easy to use and does not easily produce mistakes. After finding a line calculation graph

compatible with the engineering conditions, it is only necessary to find the position of lateral pressure coefficient ξ on the horizontal coordinates which is determined by the load sustained by the actual engineering. We use this point as the vertical line which intersects with each d_i (or β_i) line and then the longitudinal coordinate of each intersecting point is the bending moment coefficient (or axial force coefficient). Afterwards, based on formula (7), we can calculate each bending moment and axial force and make bending force and axial force graphs. Because the line calculation graphs clearly show the most non-advantageous sectional positions and the sizes of their internal force coefficients, it is very convenient when carrying out sectional strength checking. Because one can at one glance see the most non-advantageous sectional position, it is only necessary to directly check compute the most non-advantageous sectional strength. It is unnecessary to individually calculate each section's internal force to determine the most non-advantageous sectional positions. Therefore, it raises the work efficiency to a relatively large extent but does not easily produce errors. At present, although many structure handbooks such as Reference [28] etc. separately give the vault and springer bending moment coefficients under vertical and lateral load effects, during use it is necessary to superpose the bending moment coefficients of the two types of loads and also additionally calculate the axial force coefficient which is still quite troublesome. Based on the energy method, Qinghua University used the computer calculated "Straight Wall Arch Shape Lining Static Calculation Table" etc. [21,29] and although they overcame the above drawback yet it was only suitable for situations with vertical and uniform load effects. However, in actual engineering, most have lateral load effects and so it is also necessary to do additional calculations for this type of situation.

(2) The line calculation method has more control over the section and it easily and accurately determines the non-advantageous sectional positions. This is beneficial to correct

design and for avoiding unsafe factors. Generally, the structural data only give the internal force coefficients of one to two sections yet these two sections (vault and springer) are usually not dangerous sections. For example, for a double hinged semi-circular drop arch under vertical evenly distributed load many references only give vault bending moment $M_o=0.0189ql^2$. In reality, the maximum bending moment is on the section of hance $\varphi=65°$, $M_{max}=0.0225ql^2$. Based on $M_{67.5°}= -0.0223ql^2$ consulted from the line calculation method, the errors are much smaller as compared to the latter. In the example of calculating the straight wall semi-circular arch given in Reference [26], after calculating the internal force and eccentric distance of the vault and springer, they determined that the most non-advantageous section on the arch was in the vault (its bending moment was 0.38 ton meters, axial force 17.14 tons, eccentric distance 0.0222 meters) and based on this carried out strength checking. However, when using the line calculation graph with one glance we can see that the danger section is in the vicinity of the $\varphi=67.5°$ section, its bending moment is 1.367 tons, axial force 26.54 tons and the eccentric distance is -0.0515 meters which is much larger than the eccentric distance of the vault. By using this checking, they could get relatively close to the non-advantageous section and avoid the unsafe factors.

(3) It can comprehensively compare the sizes of each section's internal force and their overall distribution and correctly determine whether or not the designed section is truly optimized thus avoiding onesidedness in the analysis of the advantages and disadvantages of a certain section. For example, we can clearly see from Fig. 10 that when vector-span ratio f'=0.5 and rise-span ratio h'-0.65, it is relatively suitable for lateral pressure coefficient $\xi=0.35$. Because of this time the bending moment of each section is relatively small and the distribution is relatively uniform, when ξ is too large or too

small this causes the bending moments of several sections to become large and the distribution to be uneven. The larger the deviation the more non-advantageous it is. However, some references [1,14,15,19] only researched the change patterns of the vault section's bending moment and eccentric distance thus obtaining the conclusion of "decreasing the rise-span ratio and enlarging the vector-span ratio can reduce the internal force and eccentric distance of the section and thus raise the structural bearing force." This is quite unconvincing because under certain conditions, although the vault's bending moment coefficient a decreases with the increases of f' (Fig. 11), yet when f' is further enlarged the vault's bending moment coefficient becomes zero or a negative value. When a negative value, the absolute value of the vault's bending moment coefficient increases with the increases of f' and in the same way this is not advantageous. Even more important is the fact that even if the bending moment of the vault section decreases, the bending moment coefficients of other sections (hance, springer, wall etc.) possibly increase. In reality, the bending moment coefficient of the control section does not necssarily decrease because the control section is not necessarily on the vault. After considering the change patterns of the section's internal force, we can obtain a maximum bending moment coefficient change pattern curve such as the a_{max} curve in Fig. 11. This curve has a minimum value and this area's corresponding vector-span ratio f' is the optimized vector-span ratio (in Fig. 11, $f'_{optimized}$ =1/2.5). We can see from this that when ξ and h' are fixed it is necessary to have a corresponding optimal vector-span ratio $f'_{optimized}$. On the contrary, when ξ and f' are fixed, we can also find an optimal rise-span ratio $h'_{optimized}$. Both f 'and h' can be obtained using the line calculation graph.

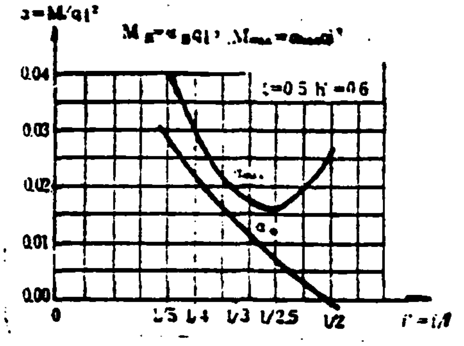

Fig. 11 Relational chart of straight wall circular vault's bending moment and the maximum bending moment of each section which changes with the vector-span ratio.

The above mentioned use of the line calculation diagram as a method to determine the rational proportion dimensions between the load distribution and the rise-span ratio and vector-span ratio is not only suitable for situations without elastic resistance but it is also suitable for situations with elastic resistance. Using the computer calculated results which employed the chain rod method as an example [30], when ξ =1/4, h'=0.8 and f'=1/2-1/5, the influence of the elastic resistance is as shown in Fig. 12 and the non-dimensional coefficient (Kl^4/EJ) indicates the influence of the elastic resistance. (In the expression, K is the strata elastic resistance coefficient, l is the calculated span, E is the structural material's elastic module and J is the section's moment of inertia). The larger this coefficient the greater the influence of the elastic resistance. Following the enlargement of Kl^4/EJ, the maximum bending moment coefficient of the section correspondingly decreases yet the position of the optimal vector-span ratio (or rise-span ratio) does not change. We can see from Fig. 12 that when there is no elastic resistance (at this time, $Kl^4/EJ=0$), $f'_{optimized}=1/2$ and following the enlargement of Kl^4/EJ, $f'_{optimized}$ is then 1/2. However, the maximum bending moment coefficients of the various vector-span ratios gradually become

close to eachother. This shows that elastic resistance has beneficial effects on the structure. It can cause the non-optimized arch shape to tend towards optimization yet it is unable to cause the stress properties of already optimized arch shapes to deteriorate. In certain situations wherein the elastic resistance causes the optimized arch shape to be changeable they then do not coincide with reality because of the assumptions of the elastic resistance distribution range and the distribution graph. Moreover, there is also a certain discrepancy between using the local deformation theory solution and actual entire deformation thus causing the calculation results to be reatlively disorganized.

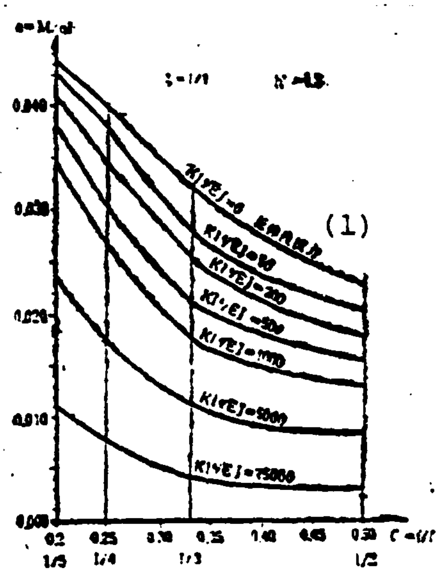

Fig. 12 Influence of Kl^4/EJ on the maximum bending moment coefficient of sections.

Key: (1) Without elastic resistance.

(4) Based on the conditions of actual arch shapes of constructed sites and their destruction, we can use the line calculation graph to deduce the load distribution so as to estimate the real lateral pressure coefficient of the strata. This

provides strata analogous materials for engineering rebuilding and continued building and we can also accumulate data for the study of the strata lateral pressure coefficient. See the section on engineering examples for its method.

3. Design Method of the Straight Wall Lining Optimized Arch Shape

The wall area of the straight wall lining is rectilinear and the shape of the arch area was also first determined such as the straight wall circular arch, straight wall elliptic arch, straight wall parabolic arch etc. Therefore, the optimized arch shape design of the straight wall lining is in essence the problem of selecting the optimized vector-span ratio or optimized rise-span ration.

We can know from the line calculation graph that we must have an optimized vector-span ratio $f'_{optimized}$ corresponding to certain ξ and h'. Therefore, each line calculation graph can draw an optimized point on the (ξ ,h') coordinate system and the many optimized points obtained from the same type of line calculation graph can induce an optimized curve. The many optimized curves form a complete selection chart for rational dimensions for the straight wall lining optimized arch shape. For example, Fig. 13 is the selection chart for the key elements of the constant section straight wall circular arch's optimized arch shape. When used, based on lateral pressure coefficient ξ and rise-span ratio h' we can find optimized vector-span ratio $f'_{optimized}$; or based on $\xi \cdot f'$ we can find optimized rise-span ratio $h'_{optimized}$; we can also obtain many paired optimized arch shape key elements f' and h' based on a known lateral pressure coefficient ξ for use in the selection plan.

Because elastic resistance which is beneficial to arch shape optimization causes the optimization range to enlarge for a cave room built under conditions where relatively small ξ can supply

relatively large elastic resistance, its optimized arch shape's key element values allowed suitable offset. When the quality of the surrounding rock is good, the allowed optimized vector-span ratio or rise-span ratio of the cave room is appropriately lowered. Yet, this is very non-advantageous for tunnels with poor soil quality and large ξ and when the deviation of the optimized point is too large. At the same time, we should also pay attention that for cave rooms with small vector-span ratios constructed in poor land areas, it is necessary to use side tunnelling, side reinforcing, consolidation at every step etc. construction measures so as to prevent the occurrence of cave-ins.

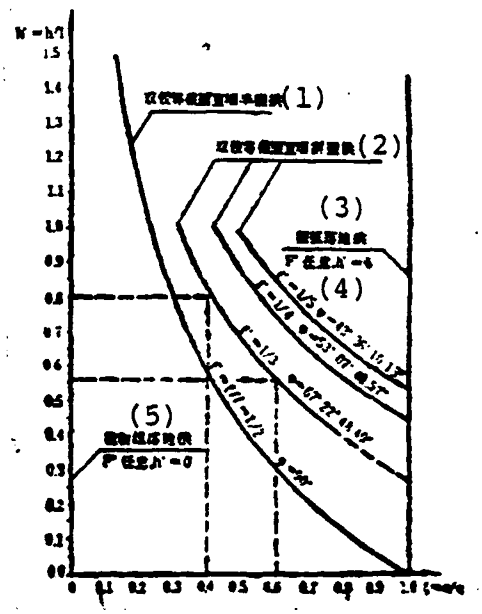

Fig. 13 Selection chart for the optimized arch shape's key elements of the straight wall circular arch and drop arch.

Key: (1) Double-hinged constant section straight wall semi-circular arch; (2) Double-hinged constant section straight wall cyclotomic arch; (3) Circular arc drop arch; (4) Arbitrary; (5) Parabolic drop arch.

Example 3: a certain straight wall circular arch structure sustains a vertical and uniform load of 12 tons/meter^2 and the lateral equally distributed load is 4.8 tons/meter^2. If we select a wall height of 1.6 meters and the calculated span is 2 meters we attempt to determine its optimized vector-span ratio and calculate its internal force and eccentric distance. At the same time, we compare it with the eccentric distance of a non-optimized arch shape.

The solution of ξ =e/q=4.8/12=0.4, h'=h/l=1.6/2=0.8 is looked up from Fig. 13. ξ =0.4 is taken as the vertical line, h'-0.8 is taken as the horizontal line, the two lines intersect at one point and therefore the point is located near the f' $\approx$1/3 line and we obtain $f'_{optimized}$=1/3. We further look up the line calculation graph of the double hinged straight wall cyclotomic arch with n=1 (constant section), f'=1/3, h'=0.8 (Fig. 14) and obtain a_i and β_i. Thus, we can calculate the internal force of each section as shown in Table 1.

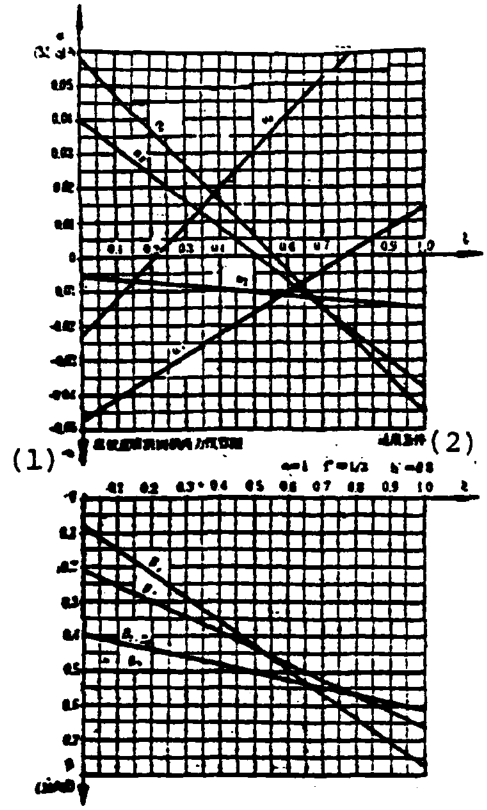

Fig. 14 Key: (1) Line calculation graph of the internal force of the double hinged straight wall cyclotomic arch; (2) Usable conditions.

(1) 截面号	内力(2)	(7) 弯矩M(吨米) (8) 弯矩系数α_i	(9) 弯矩 = $\alpha_i ql^2$	(10) 轴力N (吨) (11) 轴力系数β_i	(12) 轴力 = $\beta_i ql$	偏心距(米) (13) $e = M/N$
1	拱顶 (3)	0.0162	+0.777	0.36	8.64	+0.09
2		0.0080	+0.384	0.39	9.36	+0.041
3	拱腰 (4)	-0.0100	-0.480	0.49	11.76	-0.041
4	拱脚 (5)	-0.0230	-1.105	0.49	11.76	-0.094
5	墙中 (6)	0.0200	+0.960	0.50	12.00	+0.080

(14) 表中：$ql^2 = 12 \times 2^2 = 48$吨米 $ql = 12 \times 2 = 24$吨

Table 1 Internal force calculation table. (continued next page)

Table 1 (continued)

Key: (1) Section number; (2) Internal force; (3) Vault; (4) Hance; (5) Springer; (6) Wall; (7) Bending moment M (ton meters): (8) Bending moment coefficient; (9) Bending moment; (10) Axial force N (tons): (11) Axial force coefficient; (12) Axial force; (13) Eccentric distance (meters); (14) In the table: ql^2=12x2=48 ton meters, ql =12x2=24 tons.

Therefore, when we use the optimized vector-span ratio $f'_{optimized}=1/3$, e_{max}=9.4cm is springer 4. In the same way we can obtain:

When f'=1/2, e_{max}=13.4cm is at wall 5 point;

When f'=1/4, e_{max}=15.2cm is at springer 4 point;

When f'=1/5, e_{max}=18.6cm is at springer 4 point.

By comparing we can know that when f' is 1/3 it is optimal, its eccentric distance is about twice as small as when f'=1/5 and therefore the thickness of the section can also be correspondingly thinner.

Example 4: the covering soil of a certain underground passage is relatively shallow. In order to increase the depth of the covering soil, satisfy the employed clearance requirements and consider the construction convenience etc., we determined that the straight wall cyclotomic arch structure used a vector-span ratio of 1/3 and we test selected its optimized rise-span ratio. If, based on the utilization requirements, the wall height was 1.8 meters, what was its optimized span? Further, was the relatively reduced span economical?

It is known that q=8.7 tons/meter^2, e=4.87 tons/meter^2, $\therefore \xi$ =e/q=0.56, f'=1/3, h=1.8 meters.

Solution: based on ξ =0.56 and f'=1/3, we can look up from Fig. 13 that optimized rise-span ratio $h_{optimized}$=0.6,

$\therefore$ optimized span $l=h/h'_{optimized}=1.8/0.6=3$ meters.

By checking the line calculation graph (Fig. 15), we find that a_{max} 0.017 is at the springer and its corresponding axial force coefficient $\beta_{max}=0.5$

$$e_{max}=\frac{a_{max}}{\beta_{max}}\cdot l=0.017\times 3/0.5=0.102米$$

Key: (1) Meters.

If arch thickness d=0.25 meters and number 200 concrete R-160 tons/meter^2, then $0.45d=0.1125$ meters $> e_{max}=0.102$ meters $> 0.2d=0.06$ meters.

$$K=\frac{1.75R\cdot b\cdot d}{N\left(\frac{6e_{max}}{d}-1\right)}=$$

$$\frac{1.75\times 160\times 1\times 0.25}{0.5\times 8.7\times 3\left(\frac{6\times 0.102}{0.25}-1\right)}=3.7>3.6(可)\ (1)$$

Key: (1) Can.

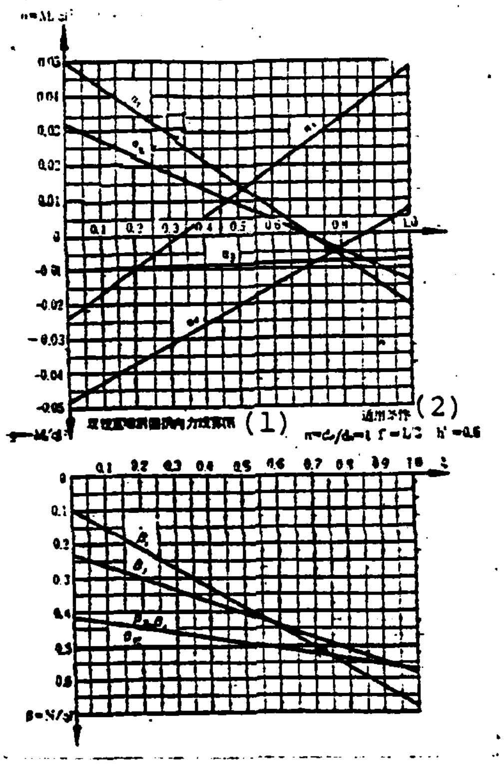

Fig. 15

Key: (1) Line calculation graph of the internal force of the double hinged straight wall cyclotomic arch; (2) Usable conditions.

If we use a 2 meter span, we assume the load is ξ=0.56, h'=h/1-1.8/2=0.9 looked up in the line calculation graph (sketch) we obtain

$\alpha_{max} = 0.0505$ $\quad$ $\beta_{max} = 0.5$ (在墙中)(1)

$\therefore M_{max} = \alpha_{max} q l^2 = 0.0505 \times 8.7 \times 2^2 = 1.757$ 吨米 (2)

$N_{max} = \beta_{max} q l + d \cdot h \cdot \gamma / 2 = 0.5 \times 8.7 \times 2 + 0.32 \times 1.8 \times 2.3/2 = 9.36$ 吨(3)

Key: (1) In the wall; (2) Ton meters; (3) Tons.

The rear part calculated from the axial force is the wall's dead weight above the middle of the wall, the wall thickness selects 0.32 meters and the capacity of the concrete is γ=2.3 tons/meter^3.

$$\therefore e_{max} = M_{max}/N_{max} = 1.757/9.36 = 0.1877 \text{(1)} >$$

$$0.45d = 0.144 \text{(2)}$$

$$K = \frac{1.75 \times 160 \times 0.32}{9.36\left(\frac{6 \times 0.1877}{0.32} - 1\right)} = 3.8 > 3.6$$

Key: (1)-(2) Meters

Attention: when the span is 2 meters, d is taken as 0.32 meters. Although the safety coefficient is sufficient yet the eccentric distance is too large and we should increase the thickness and recalculate. However, even though this be the case, we can see that under the same safety coefficient conditions, because we used the optimized arch shape dimensions, the span enlarged 1 meter but the thickness became 21.9% thinner. We can thus see that it has marked economic effects.

III. Examples of Engineering Applications

Theory stems from practice and it is only necessary to return to practice to receive the test of practice. Below, we will enumerate several examples of utilization so as to explain the utilization methods and real effects.

(1) Use of the optimized arch shape design resolves the problem of "incessant cracks" which has been unable to be solved over the last nine years and it also raises engineering quality.

The entrance of tunnel engineering at Yuanmaoshan is located in a poor geological area and the original design was the straight wall three-centered pointed arch. After construction began in 1971, beginning at a distance 60 meters from the cave opening there was widespread cracking in the hance area and the

cracks continually pushed forward with the progress of the construction. For this reason "consultations" by related departments were requested many times and they made every effort to halt the cracks. They first increased the structural thickness; it was necessary to reduce overbreaking as much as possible and the essential backfill of the overbreak was dense; the transverse arch shaped boards put up in the lining stopped the cracks from advancing; local reinforcement; they raised the grade of concrete, strengthened the curing and prolonged the form removal time; and prohibited blasting shock etc. measures. The result was that they were to no avail. Under these conditions, in September of 1980, this unit invited us to the site to give counsel. Based on the actual crack conditions, we deduced the lateral pressure coefficient and based on this designed three optimized arch shape plans. In November, we decided on the third plan of construction based on the most convenient construction even though the optimized performance was relatively poor. As expected, the cracking stopped and not only was the structural thickness 10% thinner than the original plan but moreover it withstood the tests of blasts in the cave. To date (this paper was written in September, 1981), there has not been cracking in over 200 days. We will now briefly present the design steps:

1. On-the-spot examinations of crack destruction of constructed sections. The examinations showed that: aside from the 60 meter tunnel opening, the hance section had widespread cracking and the crack width varied from 0.3-5cm. The crack area geneally changed between the hance and the springer (points 3-4 in Fig. 16). The vault section of the local area (between points 0-1) was crushed and pieces fell yet the majority of the vault section did not have macroscopic destruction. For the area where the vault had crushed and fallen to pieces, its hance cracking was relatively serious.

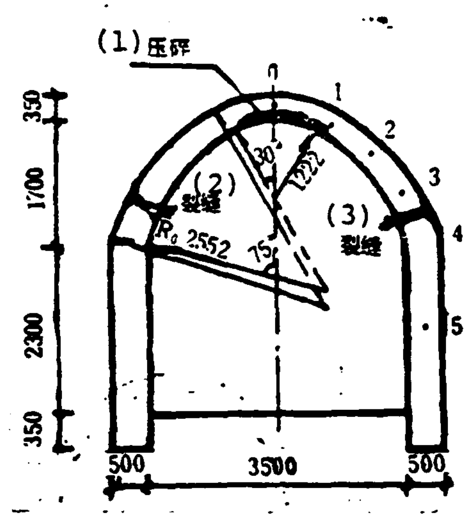

Fig. 16 Constructed tunnel dimensions and destruction areas.
Key: (1) Crushed; (2)-(3) Cracking.

2. Deducing the Lateral Pressure Coefficient

Based on the actual dimensions and arch shape etc. of the construction engineering, we can make a bending moment line calculation graph of this engineering (Fig. 17). We can see from the graph that when $\xi = 0.48$, the bending moment of the vault begins to change from a positive bending moment to a negative bending moment and the crushing of the inner rim of the vault is the result of a negative bending moment. Therefore, we can determine that ξ is certainly larger than 0.48 yet how large after all is ξ? We can know from section checking that the design standards generally do not allow the eccentric distance to be greater than 0.45d because when $|e| \geqslant 0.45d$, it is easily destroyed and it is also easily destroyed when $al/\beta \geqslant 0.45d$. It is already known that this tunnel's 1-4 meters, d=0.35 meters (using the arch's minimum thickness value), β can be looked up in the axial force line calculation graph based on the estimated ξ value ($\xi > 0.48$) and when ξ is relatively large we can approximate that β is 0.5. In this way, we can estimate that when destruction is produced the minimum

absolute value of the bending moment coefficient is $|a| \geqslant 0.45d \cdot \beta/1 = 0.45 \times 0.35 \times 0.5/4 = 0.197$. This shows that when bending moment coefficient a is larger than or equal to 0.197, the arch can produce destruction.

When $\xi = 0.5$, $a_4 = 0.02 > 0.0197$ (Fig. 17). This shows that at this time hance point 4 area possibly sustains positive bending moment and the inner rim cracks. Under equal thickness point 6 in the wall also has inner rim tensile cracking yet the wall area in the actual engineering is very thick and did not have cracking so we did not make a control point (the same as below). Each of the other points a were smaller than 0.0197 and generally did not have cracking.

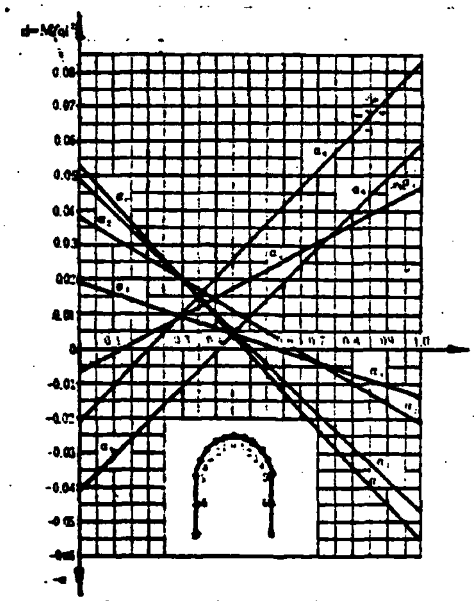

Fig. 17 Bending moment line calculation graph of constructed tunnel.

When ξ is increased to 0.65, a_0 and a_4 are both larger than 0.0197. MOreover, point 0 (vault) is the negative bending moment, point 4 (hance) sustains positive bending moment (Fig. 17) and therefore, at this time, the vault has inner rim crushing

and the hance has inner rim tensile cracking.

When ξ further increases to 0.73, a_5 and a_4 are equal and both are larger than 0.0197. This shows that the inner cracking location will gradually shift from the hance to the springer. Because the structural thickness and construction mass are different, the inner rim cracking of the arch can also occur in the hance as well as the springer and even in both locations. At this time, a_2 is also larger than 0.0197 yet $a_1 < a_0$ which explains that the crushing area also expands from the two sides of the vault to point 2 yet point 0 has even more serious crushing than point 1.

All three types of situations have actual engineering destruction which shows that the lateral pressure coefficients of each section are not definite values. However, the ones which appear most often are the hance's inner cracks, vault inner rim crushing or alternately non-crushing which shows that the vault is located in the critical state of destruction which is equal to the second type of situation. Therefore, we make the preliminary estimate that ξ =0.65.

3. Implementing the Optimized Arch Shape Design

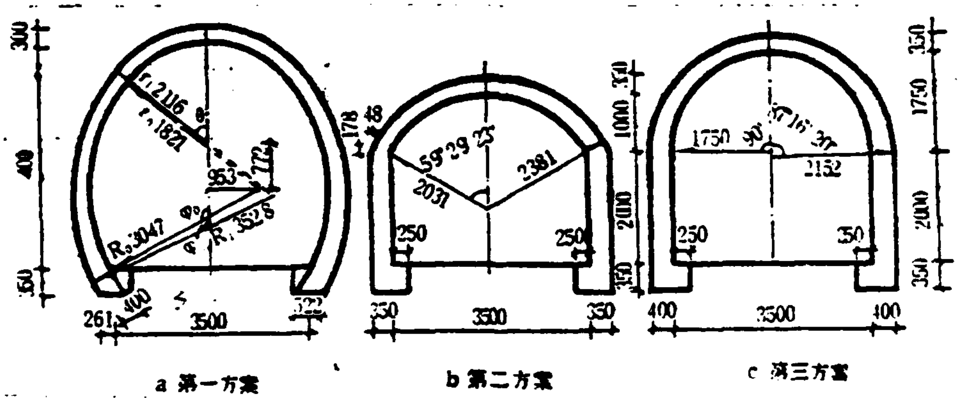

Fig. 18 Charts of the optimized arch shape design plans.
Key: (a) First plan; (b) Second plan; (c) Third plan.

Plan 1: we used the curved wall arched structure and based on ξ=0.65 and F'=4/3.5=1.1429 we refer to Fig. 6 whereby the obtained θ and φ are substituted into formula (1) and we calculate R,r,a and b as shown in Fig. 18a. The clearance of this plan coincides with the requirements, the bending moment of each section is basically zero and theoretically there cannot be cracking. The thickness is relatively thin yet the construction of the curved wall is relatively complex.

Plan 2: for convenience of construction, we used the straight wall circular arc arch (cyclotomic) plan. It was known that ξ=0.65 and based on the service requirements, the wall height was 2 meters, the wall thickness was 0.35 meters, the foundation depth was 0.35 meters and therefore $h'=(2+0.35)/(3.5+0.35)\approx 0.61$. By referring to Fig. 13, we obtain the optimized vector-span ratio $f'_{optimized}$ 1/3.5. By substituting in formula (6-1), we obtain:

$$\varphi_{optimized}=2\mathrm{arctg}2f'_{optimized}=$$

$2\mathrm{arctg}(2\times 1/3.5)\approx 59°29'23.14"$. By substituting in formula (1-1), we obtain $R=1/2\sin\varphi_{optimized}$=2.23438 meters. This plan (see Fig. 18b) of construction is simple, the bending moment of each section is relatively small and the distribution is uniform. Theoretically, it does not easily crack yet the total clear height is reduced 1 meter (the total clear height requirement is 3.75 meters) which influences utilization.

Plan 3: we used the straight wall semi-circular arch. It was known that ξ=0.65 and f'=0.5 and by referring to Fig. 13 we obtained optimized rise-span ratio $h_{optimized}$=0.38 and the optimized wall height $h=h'_{optimized}\cdot 1=0.38(3.5+0.4)=1.482$ meters which does not conform to the utilization requirements. Now, using the lowest utilization requirement of 2 meters as the designed wall height, then the designed rise-span ratio and optimized rise-span ratio have a certain discrepancy. Therefore,

the lateral wall will become thicker which will satisfy the stress requirements (Fig. 18c). The construction of this plan is the simplest and when the original arch shape changes into the present arch shape the gradually changed section is short and the wall height and total clear height satisfy the requrements yet the stress is relatively poor. Although the section's bending moment can be smaller than the original design, yet it still has a certain bending moment. It can cause the cracking to reduce yet it is unable to guarantee that cracks will not appear.

4. Testing and verifying the construction: after deciding the construction will be based on plan 3, in the interview stage the cracks have already shrunk and by the approximate optimization stage the cracks are completely eliminated. It then goes through the test of blasts in the cave and time. The third plan is only approximate optimization yet marked effects were obtained in eliminating the cracking. This shows the beneficial remedying effects of elastic resistance. It can cause the optimized range to expand yet it cannot destroy the optimized arch shape. It is only necessary that the designed arch shape and optimized arch shape be close in order to be able to attain marked effects.

(2) Use of the optimized arch shape design made the structural thickness thinner and lowered the engineering building costs. During peacetime, certain excavated underground shelters are used to hold meetings or show movies and during war they serve as shelters for people and are used to store equipment for the three defenses. The span is 20.26 meters. Because the roof of the underground shelter is used as a parking lot during peacetime, the roof has three different types of loads; the blast wave effects are the vertical and evenly distributed load, its optimized arch shape is the parabola; the optimized arch shape of the covering soil solid web static load is the catenary which

is now the open web constant load. Even if we use a suitable catenary, we can only attain several points of zero bending moment and the bending moments of the other sections are relatively small; the position of the vehicle movement load is not fixed and we must await a load design based on the influence line. It does not have an optimized arch axis. How do we obtain an optimized arch shape under constant load conditions and cause the bending moments of the above mentioned loads to be relatively small and the axial force to be relatively large under various different combined conditions? For this, we used the above "arch shape approach area" (the blackened area of $f' \leqslant 0.2$ in Fig. 6). In the arch shape approach area, the differences between the parabola, circular arc line and its corresponding catenary are relatively small and therefore the adaptability is maximum for the various loads. Even if we first select a not very suitable arch shape, yet there is slight deformation which can change the arch shape, this type of deformation does not cause structural destruction. After deformation, the arch shape and load adapt to eachother and cause the stress performance to greatly improve. Because of this, we used $f'=1/6=0.16 < 0.2$ and at the same time we determined the optimized arch shape based on the constant load. When the vehicles and blast wave loads have temporary effects, although a certain deviation is produced, yet because it is in the approach area, the bending moment is generally relatively small and the horizontal thrust is relatively large. For balanced thrust, in the design, the strata's lateral pressure is transferred to the springer of the main arch by means of the depressed arch's upright (Fig. 19). The depressed arch is also designed with a small vector-span ratio. We use the unevenness or change of an appropriate load, reduce the bending moment and at the same time increase the horizontal thrust of the depressed arch so as to bring into play the clamping support effects of the horizontal thrust on the upright and improve the upright's stress state. This type of underground shelter uses an arch shape approach area designed optimized

arch rib double curved vault and upright optimized depressed arch side wall. The mean thickness of the arch is 27cm (nearly the same span and resistance and the vault is generally 60-80cm thick, over 55% thinner) and the mean thickness of the side wall is 54cm (over 46% thinner than most design thickness). It has been used since the end of last year and the underground is often filled (728 people) with movie watchers; on the roof is often parked over ten various types of vehicles and after a 16 ton road roller rolled over it, no cracks were seen in the structure. This engineering attempt not only saved a great deal of investment capital (the actual present expenditure is 430,000 yuan) but also provided a line of thought for the concepts of prefabrication and use of factories for tunnel engineering proposed by using the "optimized arch shape approach area."

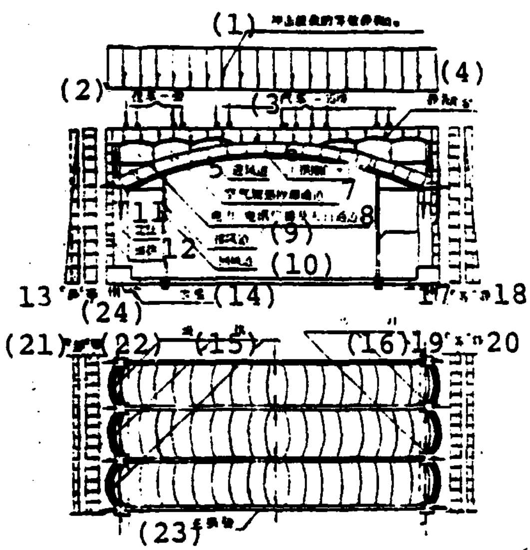

Fig. 19 Schematic of main arch ring's stress of underground shelter.

Key: (1) Equivalent static load of blast wave load; (2) Trailer; (3) Automobile; (4) Static (? illegible); (5) Air intake passage; (6) Vault ring: (7) Air heating and cooling passage; (8) Electric power, dispatch broadcasting and pedestrian passage; (9) Air exhaust paggage;

Key: (continued) (10) ? Illegible; (11) Upright; (12) Depressed arch; (13) Static; (14) Rock rail; (15) Depressed arch; (16) Upright; (17) Equal; (18) Static; (19) Equal; (20) Static; (21) Static; (22) Equal; (23) Main arch rib; (24) Equal.

(3) Based on the calculation results for the optimized arch shape, we will discuss the rationality of the curved wall standard sections of China's single line railway tunnels.

Table 2 gives a comparison of the optimal arch shape's radius and the standard design radius assuming the single line railway tunnel's curved wall lining clear rise F_o=1.65+0.85-7 meters, clear span l_o-4.9 meters and clear vector-span ratio F'_o=1.4286 when lateral pressure coefficient ξ changes between 0.2-0.7.

比较项目及 (1) 截面位置	标准设计半径 (5) (米)		(8) 优化设计半径					
			(9) 侧压力系数$\xi = e/q$					
	(6)修改前	(7)修改后	0.2	0.3	0.4	0.5	0.6	0.7
(2) r_0(拱顶部分)	(0°~30°) 1.82	(0°~45°) 2.22	(0°~65.9°) 1.69	(0°~61.3°) 1.95	(0°~57.7°) 2.23	(0°~54.7°) 2.49	(0°~52.2°) 2.78	(0°~50.1°) 3.06
(3) R_0(拱腰部分)	(30°~75°) 3.52	(45°~78°51′) 3.21						
(4) R_0'(曲墙部分)	(>75°) 7.47	(>78°51′) 8.13	(>65.9°) 11.38	(>61.3°) 8.16	(>57.7°) 6.82	(>54.7°) 5.72	(>52.2°) 5.13	(>50.1°) 4.70

Table 2 Comparison of standard design radius and optimized radius.

Key: (1) Compared item and section position; (2) Vault section; (3) Hance section; (4) Curved wall section; (5) Standard design radius (meters); (6) Before modifications; (7) After modifications; (8) Optimized design radius; (9) Lateral pressure coefficient.

Analysis: in the past, the inner contour design radius of curved wall structure standard sections for China's single line railway tunnels was: when the section is located from vault ($\gamma=0°$) to $\gamma=30°$, $r_o=1.62$ meters; when $\gamma=30°-75°$, $R_o=3.52$ meters; when γ shifts from 75° to the springer, $R'_o=7.47$ meters. From the point of view of its radius of curvature, this type of arch shape is only suitable when lateral pressure coefficient $\xi \leqslant 0.2$ because its radius of curvature is relatively close to the optimized radius calculated in Table 2. By comparing it with the optimized radius when $\xi=0.2$, we can see that when the section is located at 0°-30°, the radii of the two are separately 1.62 meters and 1.69 meters which is very close. When the section is located in 65.9° to the springer, the optimized design radius is 11.4 meters and the standard design radius is 7.5 meters. The standard design radius of this section is relatively small which shows that the lateral pressure resistance capabilities of the side wall section of the single line tunnel's curved wall structure standard section are relatively strong. However, in the hance section with $\gamma=30°-65.9°$, the optimized radius is 1.69 meters and the standard design is 3.52 meters which shows that this section's radius has become larger and its ability to resist lateral pressure has become smaller. A radius area which tends to be large easily produces the destruction of inner rim tensile cracking and practice has proven this point. The investigation results of 1972 on railway tunnel cracking throughout China showed that most of the cracks were produced on the inner side of the hance at a 45° included angle with the vault. This point is identical to the theoretical calculation results - inner side cracks easily occur at 30°-65.9° with the vault. The above is only related to situations with relatively small laterial pressure ($\xi=0.2$), for example, what will the situation be after the laterial pressure increases? In the 30°-0° arc section, the radius still tends to be large and internal cracking is possible. However, following the increase of ξ, the arc section range of 30°-0° can become smaller and smaller and the difference between

the radii of the two gradually reduces. The possibility of internal cracking in this section gradually lessens. However, the standard design radius of the vault section (0°-30° area) tends to be small and the larger the increase of the lateral pressure the larger the disparity. This shows that when the lateral pressure increases, because the vault's standard design radius is very small (very pointed), it easily produces outer side cracks on the vault and the destruction of inner side crushing due to the effects of the negative bending moment. At the same time, θ shifts to the springer section because the larger the standard design radius the more the relative tendency to be large. This section can also produce internal cracks. Therefore, we can conclude that: from the point of view of the optimized arch shape, when the lateral pressure coefficient is relatively small, the original standard design section only produces internal cracks in the hance; when the lateral pressure coefficient is medium, aside from the internal cracks of the hance, it can also produce slight inner rim crushing on the vault; when the lateral pressure coefficient is relatively large, the inner rim crushing of the vault gradually becomes more serious and the internal cracks of the hance shift downwards to the arch toes or wall section. In actual engineering, many inner side cracks are produced in the hance as well as the typical destruction of inner side crushing of the vault. This shows that the original standard design section's vault is very pointed (the curvature is too large, that is, the radius of the curvature is too small) and the hance is too depressed (the radius of the curvature tends to be large). Therefore, when the lateral pressure coefficient is larger than 0.2 (in reality, they are generally all larger than this value), it is not very suitable to use the original standard design curved wall three-centered pointed arch. Based on the investigative research of cracks in alreay constructed engineering, some materials propose changing the vault of the single line tunnel into a semi-circular or close to semi-circular three-centered arch. It is better for the double

line tunnel to use an arch axis more level than the original arch axis [2] and it is not advantageous for the curvature of the vault to be too large. The flat vault and curvilinear side wall lining and other proposals worth recommending [31] are suitable for commonly seen loess strata. The standard sections of railways have also made modifications in this area (Table 2). After modifications, the vault became level (the radius was enlarged) and the radius of the hance became small. It is doubtful that this is a large improvement causing the stress condition to have a relatively large change for the better. By comparing the data in Table 2, we can see that after these types of modifications, the arch shape is relatively suitable for strata with ξ =0.3-0.4. Yet, in most situations, in the hance range of 45°-0°, the radius still tends to be large, the radius is not much larger and the influencing effects are much weaker. The other sections also have certain disparities but the disparities are relatively small. Therefore, the possibility of producing destruction is also greatly reduced. However, when the lateral pressure coefficient is much larger than 0.4 or the roof is the saddle load effect, different dangers of destruction still appear. Therefore, the tunnel's standard design chart should be worked out based on the different lateral pressure coefficients. In situations with relatively large bias or non-uniform loads, it is also necessary to carry out additional design. No matter what the surrounding rock pressure and its distribution are, aside from the differences of the curved walls and straight walls, the integrated use of one type of arch shape appears to be improper.

Because of the limitation of space, we will not go into detail on the applications of the optimized arch shape design theory in analyzing the destruction mechanism of surrounding rock, in analyzing cave room stability and destruction locations as well as in guiding construction.

IV. Conclusion

The optimized arch shape design which can cause arch structures to be economical and rational is one important link in the faster and more economical development of underground arch architecture. When synthesizing the existing research achievements, the optimized arch shape under commonly seen load effects is already basically understood. For example, under vertical uniformly distributed loads, the optimized arch shape is the parabola; under radial uniformly distributed load effects or equal vertical and horizontal uniformly distributed loads, the optimized arch shape is the single centered circle; under vertical saddle load effects (i.e. the solid-web arch load), the optimized arch is the catenary with different arch axis coefficients; when the vertical and horizontal uniformly distributed loads have simultaneous effects and the two are made up of different proportions, the optimized arch shape is the three-centered circle with optimized arch shape key elements (F', θ and φ). When the requirements are designed based on the straight wall circular arc arch, we can select the optimized vector-span ratio or optimized rise-span ratio based on the selection graph of the straight wall circular arch's optimized arch shape key elements so as to use rational proportion dimensions to approach the optimized arch shape. The straight wall elliptic arch and straight wall parabolic arch can also refer to a similar method to determine the optimized arch shape.

The common laws of the optimized arch shape are: (1) the direction with large pressure should project outwards - become pointed; the direction with small pressure should contract in towards the inside - become level. We can perhaps say that the elliptic long axis should be the same as the maximum pressure direction, that is, when the roof pressure is large the cave should be high; when the lateral pressure is large the cave should be flat. If a high and narrow cave room is under the

effects of relatively large lateral pressure, the inner rim of the roof area is crushed and collapses and the floor bulges up. Based on the principle of the optimized arch shape, increasing the width of the cave causes the cave to become flat and often the cave becomes stable. This is the same as the conclusion of stress control technology [31]. (2) The load distribution is closely linked with each curvature of the optimized arch shape: in the maximum load direction, the curvature should be maximum; in the middle position of the load, the curvature takes second place; in positions with minimum or no load, it is beneficial for the curvature to be minimum or designed as a straight line. When the position of the load and curvature do not adapt to eachother and the internal force exceeds the allowable strength of the material, destruction will be produced. Pointed arch areas with excessively large curvatures easily create inner rim crushing and collapse after enduring negative bending moment and it is beneficial to enlarge its radius of curvature (i.e. reduce the curvature); level and flat areas with excessively small curvatures easily produce inner rim cracks after enduring positive bending moment and we should enlarge the curvature of this area (i.e. shrink the radius of the curvature).

In investigating the rational section shape of underground cave rooms: one is based on the elastic theory. We take as the starting point that the periphery of the cave room does not produce tensile stress and each section only affects relatively small toroidal pressure stress. One is based on deductions from the structural mechanics theory. We take as the starting point that each section of the bearing arch does not produce bending moment or only produces relatively small bending moment and the bending moment distribution of each section is relatively uniform. We add on the initial conditions of the two which are not completely the same: for the former, based on the four-sided stress and the entire section's sealed cave form, the focus of consideration is the problem of tunnel surrounding rock

destruction; for the latter, based on the three-sided stress and the non-sealed lining, the focus of consideration is the problem of the supporting structure destruction. Therefore, under certain specific conditions, although the conclusions have areas of similarity, yet they are not completely the same.

When $\xi=0$, from calculations based on the elastic principle, the vault always sustains tensile stress and is not in the rational section form; but in view of the structurl mechanics, its optimized arch shape is parabolic.

When $\xi>0$, the two prove that the optimized arch shape is elliptic and the elliptic long axis should be the same as the maximum pressure direction. However, the elastic theory considers that it should be a complete ellipse with $A/B-e/q=\xi$ and structural mechanics considers that it is an ellipse with $A/B=\sqrt{e/q}=\sqrt{\xi}$ or a certain part of this ellipse. For example: when $\xi=1/4$, if it is required to use a width of 2 meters, then the rational section of the former will be a complete ellipse with a short axis of 2 meters and a long axis of 8 meters. At this time, one half of the height cannot be used. However, the latter is a part of an ellipse with a short axis of 2 meters and a long axis of 4 meters. Its height can be determined by the utilization requirements and be completely used (Fig. 20). Therefore, the difference between the two is relatively large. For the moment, we will not discuss which type is closer to reality but wait for a large amount of future practices for proof. However, there is one point we can explain: the rational section of the elastic theory must be completely elliptic and moreover the ratio of its long and short axes is only related to ξ and we are still unable to consider the utilization conditions. Therefore, its space use coefficient is very low. A large amount of unnecessary peripheral reinforcing instead caused the "rational section" to be even more wasteful than the non-rational section. Therefore, it is often difficult to

implement in actual engineering. In special situations, when $\xi=1$, the theories of the two completely coincide and separately prove that the optimized arch shape is an isometric ellipse with A/B=1 (i.e. a circle or part of a circle).

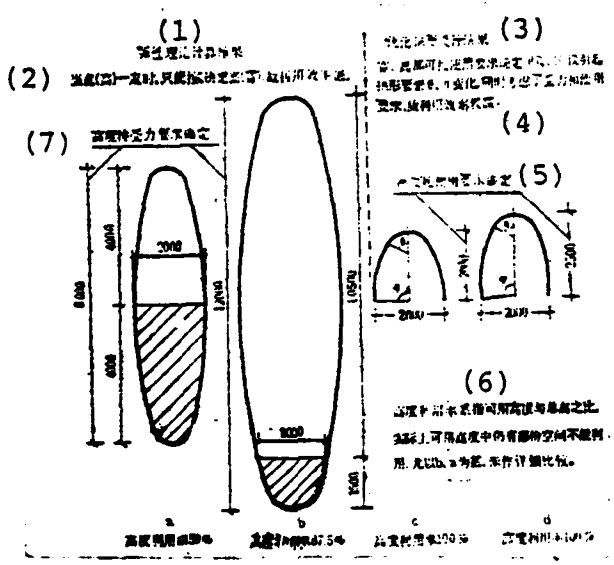

Fig. 20 Optimized arch shape when $\xi=1/4$ and the width is 2 meters.

Key: (a)-(d) Height utilization rate; (1) Elastic theory calculation results; (2) When the width (height) is fixed, we can only determine the height based on ξ and therefore the utilization rate is low; (3) Optimized arch shape design results; (4) The width and height can be determined based on the service requirements and ξ and (illegible) only introduce the changes of the arch shape's key elements θ and q. At the same time we consider the stress and service requirements and therefore the utilization rate is relatively high; (5) The height is determined based on the service requirements; (6) The height utilization rate is the ratio of the usable height and total height. In reality, within the usable height there is also a section of space which cannot be used. We especially take b and a as extreme and have not yet made detailed comparisons; (7) The height is determined based on the stress requirements.

As regards the problem of the optimized arch shape with straight wall lining, the elastic theory only studied certain

known sections and did not attain widespread regularity. Moreover, the premise of the theory is a complete, continuous, uniform elastomer with each direction the same but in reality the theory and practice are unable to satisfactorily coincide. Therefore, this paper focused on the method of structural mechanics to investigate the rationality of the shape of the structural section. Because we are limited we have only made a few commonplace remarks by way of introduction so that others can present some valuable opinions. Readers are requested to correct the inappropriate statements made.

Main References

[1] C.C. Daweiduofu, The Calculation and Design of Underground Structures, Higher Education Press, First Edition Dec.1957.

[2] Technological Information Office of the National Architecture Committee's Architectural Science Academy, Compilation of Technical Materials on Loess Underground Architecture, Nov., 1972.

[3] Shirokei Shoni, Introduction to the Investigation of Deformation of Japan's Nationally Run Railway Tunnels and Renovation Experiences, Collected Translations on Tunnels, Dec., 1980.

[4] Kasitenai, Tunnels and Tunnel Statics, Shanghai Science and Technology Press, First Edition, Feb., 1980.

[5] Gao Lei et al, Mine Rock Mechanics, Metallurgy Industry Press, First Edition, July, 1979.

[6] Compilation Group on Tunnel Engineering of the Lanzhou Railway College, Tunnel Engineering, People's Railway Press, May, 1977.

[7] B.M. Mositekefu, Large Section Underground Structures, China Architecture Industry Press, First Edition, August, 1980.

[8] Mechanics Laboratory of the Xian College of Metallurgy and Architecture, Photoelastic Test Research on Loess Area Mountain Pressure, Nov. , 1975.

[9] Gu Jincai et al, "Destruction Morphology of Several Types of Cave Rooms in Geological Materials, (Small Scale Test Results)," Shelter Engineering, No. 2,1979.

Main References (continued)

[10] Mining Simulated Test Group of Xian College of Metallurgy, Report on Simulated Tests of Loess Cave Garages, Nov., 1975.

[11] Design Research Group of Loess Double Line Tunnels of the Ministry of Railways, Summary Abstracts on Certain Loess Double Line Tunnel Tests.

[12] Liu Jingyi, "Investigation of Underground Cave Room Section Forms", Underground Engineering, No. 4, 1981.

[13] Standard Design Administrative Office of the Railway Special Design Institute, Integral Tunnel Linings, People's Railway Press, Aug., 1964.

[14] Xian College of Metallurgy and Architecture, Structural Design of Underground Factory Buildings, Aug., 1975.

[15] No. 621, Static Structural Design of Cave Garages, May 1975.

[16] Underground Architecture Engineering Teaching and Research Group of the Architectural Engineering Department of Tianjin University, Static Calculations of Underground Structures, China Architecture Industry Press, June, 1979.

[17] Railway Specialized Design Institute of the Ministry of Railways, Tunnels, People's Railway Press, June, 1962.

[18] Luo Wenbao, "Rational Design Method for Loess Cave Room Linings", Underground Engineering, Dec., 1980.

[19] Lecture at Tongji University, "Underground Architectural Engineering", Aug., 1968.

[20] Second Design Institute of Ministry of Railways, Tunnels, People's Railway Press, First Edition, June, 1978.

[21] Huainan Institute of Coal and Shandong Institute of Mining, Mine Building Architectural Structures, Vol. 2, Coal Industry Press, First Edition, June, 1979.

[22] Agricultural Water Systems, Hydraulic Engineering Teaching and Research Group of the Wuhan College of Hydroelectric Power, Hydraulic Engineering Structures, Vol. 2, People's Education Press, Feb., 1977.

[23] Compilation Group of Engineering Mechanics of Lanzhou Railway College, Engineering Mechanics, People's Education Press, July, 1978.

[24] Mathematics Manual Compilation Group, Mathematics Manual, People's Education Press, Dec., 1979.

[25] Lin Peiyuan, "Measurements of the Strata Pressure of a Certain Double Line Tunnel on the South Section of the Beijing-Guangzhou Line and Its Results", Underground Engineering, June, 1979.

[26] Civil Air Defense Engineering Defense Materials, July, 1974.

[27] Wang Shengli, The Line Calculation Method of Internal Force of Ultrastatic Arched Structures, Dec., 1980.

[28] Underground Engineering Soil Construction Design Materials, May, 1957.

[29] Underground Architecture Teaching and Research Section of the Soil Construction Department of Qinghua University, Static Calculation Tables for Straight Wall Arch Shape Linings, Oct., 1973.

[30] Structural Dynamic Analysis Graphs of Straight Wall Vaults, Dec., 1969.

[31] Shosei Serata, "Stress Control Technology", Underground Engineering, July, 1979.

END

FILMED

5-84

DTIC